Chapter 10
Self-Assembly of Colloidal Nanoparticles on Surfaces: Towards Surface Nanopatterning

Vasileios Koutsos, John Walker, and Emmanouil Glynos

Abstract The behaviour of colloids has become an ever expanding area of research due to the increasing number of applications in both scientific and industrial fields where their unique properties are being exploited. Such areas include bio sensors, catalyst processes, microelectronics industry and drug delivery applications. In this chapter we introduce the fundamental ideas and concepts behind the reversible self-assembly of colloidal particles on solid surfaces. The emphasis is on ultrathin films, monolayers and sub-monolayers with colloidal particles of diameter of 100 nm or lower. We provide examples of three systems (colloidal silica, magnetite and high-functionality star-shaped polymers) which highlight the importance of various interactions (electrostatic, van der Waals, steric) and small scale effects (immersion capillary forces and dewetting instabilities). Furthermore, we discuss issues associated with size and softness of the nanoparticles and the different underlying physical mechanisms that govern their behaviour.

10.1 Introduction and Theoretical Background

The world of colloidal science was once an overlooked branch of chemistry that in recent years has become a multidisciplined, billion dollar industry at the cutting edge of modern research. Applications of colloidal suspensions and their adsorption onto surfaces is the basis of many industrial processes, including waste water management, paper manufacturing, the application of paints and coatings and many chemical processes.

One of the great prospects for colloidal science is the exploitation of self-assembly techniques [1–5] for surface nanopatterning. It is a term used to describe

V. Koutsos (✉) · J. Walker · E. Glynos
Institute for Materials and Processes, School of Engineering, University of Edinburgh, King's Buildings, Edinburgh EH9 3JL, UK
e-mail: vasileios.koutsos@ed.ac.uk

S. Logothetidis (ed.), *Nanostructured Materials and Their Applications*, NanoScience and Technology, DOI 10.1007/978-3-642-22227-6_10,

the ordering of systems into structures or forms without external assistance. These structures can be formed by the initial input of some energy (static systems), by the cyclical balance of chemical reactions that are initiated and eventually dissipate (dynamic) or due to pre-patterning of the underlying substrate to facilitate a desired structure (templated) [6]. It is a facile bottom-up technique and could lead to new ways of inexpensive fabrication for a variety of industrial sectors including microelectronics, photonics and biomedical applications.

The relentless drive to shrink down the scale at which devices can be manufactured has begun to approach the physical limits of what top–down manufacturing techniques can achieve; and so attention has turned to the use of bottom-up techniques [7, 8] for manufacturing in many areas of industry. Current applications of bottom up processes using self-assembly techniques include photonics [9], biosensors [10], the semiconductor industry [1, 11] and quantum dot technology [12]. Colloidal particles have been widely used as a stock material in constructing nanostructures due to their modifiable physicochemical properties [13, 14]. This has fuelled research into the behaviour of colloidal particles in suspension [15,16], their subsequent deposition or adsorption [17–19] onto a surface and their final structuring during drying [20–28].

A *colloidal suspension* (colloid) consists of a dispersed or discontinuous phase distributed uniformly throughout a dispersion or continuous medium. Disperse systems where all the particles are of a similar dimension are known as monodisperse, and systems where the particles are present in a range of sizes are referred to as polydisperse. For the majority of colloidal materials the size of the dispersed medium lies in the dimension range of 1–1,000 nm, although this is not a set limit to define a colloidal system. This range of scale gives colloidal systems one of its defining characteristics, a larger surface area to volume ratio at the dispersed phase. Therefore it is the interfacial properties between the dispersed and continuous mediums that play a dominant role in determining the behaviour of a colloidal system.

It is normally desired that a colloidal suspension of particles remains dispersed and suspended within its medium. Due to their size colloidal particles are subject to random molecular collisions from the surrounding medium in a phenomenon known as Brownian motion. Such motion maintains the dispersion of the colloid particles throughout the colloidal suspension. Over time the effects of attractive forces that occur between particles will cause them to aggregate together until gravitation sedimentation occurs. In order to maintain a well-dispersed suspension, it is vital that the attractive forces between these particles be counterbalanced by repulsive ones, preventing particle aggregation.

The forces that drive self assembly could be of similar nature to the forces that govern the behaviour of colloidal particles in the suspension: electrostatic, van der Waals, steric and entropic forces. However, as the solvent evaporates some other important effects take place generating effective interactions, movement and new equilibrium (or in some cases non-equilibrium/kinetically driven) configurations. For example, in dried samples, that is, samples that involve the evaporation of the suspension, attractive capillary forces play a major role in the final structuring of

the colloidal particles (it should be noted that capillary forces can exist within liquid systems in the form of a gas bridge between two particles). In some cases, capillary forces have been shown to be responsible for particle ordering [26] whereas electrostatic interactions facilitate particle mobility within the suspension and also deposition on the substrate, but their influence on the final structure is not as pronounced [23].

10.1.1 Colloidal Particle Interactions

The most dominant forces affecting colloidal particle behaviour until the interaction distance has reached in the region of a few nanometers (where solvation/hydration forces come into play) are van der Waals, electrostatic and steric forces. The following is a concise review on these forces that have to be considered carefully when designing self-assembly systems not only in connection with particle–particle interactions but also with particle–surface interactions. It is composed from a selection of books [29–33] and other references where noted. For a more in-depth study of the range of particle–particle and particle–surface interactions it is recommended that the referenced books are considered.

10.1.2 van der Waals Forces

The van der Waals interaction between two molecules is composed of three distinct interactions that all vary with the inverse sixth power of the separation distance. The Keesom or *orientation* interaction evaluates interactions involving permanent dipole–dipole molecules, the Debye or *induction* interaction evaluates interactions between dipole-induced dipole interactions and finally the London or *dispersion* interaction evaluates the interaction between all atoms and molecules due to the quantum induced instantaneous dipole interactions. Of the three interactions the dispersion interaction component is the most important due to it always being present (while the induction and orientation interactions are dependent on the properties of the molecules). London forces can be exhibited by nonpolar molecules because of electron density fluctuations about a molecule (based on Schrödinger equation for the variation with time of the quantum state of a physical system). When an electron is on one side of the nucleus, this side becomes slightly negative; this in turn repels electrons in neighbouring atoms, making these regions slightly positive. This *induced instantaneous dipole* causes a brief electrostatic attraction between the two molecules. The electron immediately moves to another point and the electrostatic attraction is broken. Alternatively bond vibrations in molecules may produce the oscillations or they may be triggered by random, instantaneous coalescing of electrons in atoms. The electron-rich and electron-poor regions of the induced dipole may not persist for more that 10^{-14} or 10^{-15} s, but if they

can polarise the electron distribution on an adjacent molecule, electron clouds on the two molecules may begin to oscillate cooperatively with each other. The dipoles are transitory but aligned, and a net attractive force pulls the molecules together. At closer range, the oscillation becomes even more effective. The London expression for the dispersion interaction energy between two atoms or molecules is $v_L = -\frac{C_L}{r^6}$, where C_L is referred to as the London constant and depends on atomic/molecular characteristics and electromagnetic properties of the medium. Similar formulas describe the induction and orientation interactions. It is worthwhile noting that the van der Waals interactions are affected greatly by the presence of a solvent medium and also by the following: (1) The dispersion force contribution is significantly greater than that of the dipolar contribution; (2) the van der Waals interaction is significantly weakened by the presence of a solvent and (3) the dispersion force between dissimilar molecules can be attractive or repulsive. It is repulsive when the refractive index of the medium is an intermediary of the particles refractive index. For identical particles it is always attractive. Due to the fact that the period of the fluctuation in the dipoles is comparable to that of the time taken for the fluctuation to be transmitted, at long distances the dispersion energy between two atoms begins to decay even faster than $-1/r^6$, approaching $-1/r^7$ for separation distances approaching 100 nm. This phenomenon is referred to as the *retardation* effect. By assuming additivity and ignoring retardation effects, a selection of van der Waals interaction energies formulae can be derived from the integration of the interatomic van der Waals pair potential ($v_{vdW} = -C/r^6$) for sphere–sphere and sphere–surface interactions. These interaction laws are usually given in terms of the conventional Hamaker constant $A = \pi^2 C \rho_1 \rho_2$ where ρ_1 and ρ_2 are the number of atoms per unit volume in the two bodies. Typical Hamaker constants for solids and liquids in a vacuum are approximately 10^{-19} J. We note that at very short separation distances there exists a strong repulsion force generated by the overlap of the electron clouds of atoms. This force is commonly referred to as *hard core repulsion* or, for ions, the *Born repulsion*. The force is characterised by a very short range and its magnitude is rapidly increasing as the atoms approach.

10.1.3 Electrostatic Interactions

Many interfaces in an aqueous system carry an electrical charge. Interfaces with a similar charge will repel one another due to the Coulomb's law. This repulsion occurs between any "like-charge" interfaces and is an important factor in determining the colloidal behaviour of aqueous systems. Let us consider a single colloidal sphere suspended in a liquid medium. At the interface between the surface of the particle and the liquid we will assume any charged surface to be uniformly charged. Each colloid carries a "like" electrical charge which produces a force of mutual electrostatic repulsion between adjacent particles. The charging of a surface in a liquid can originate from either the ionisation or dissociation of surface groups

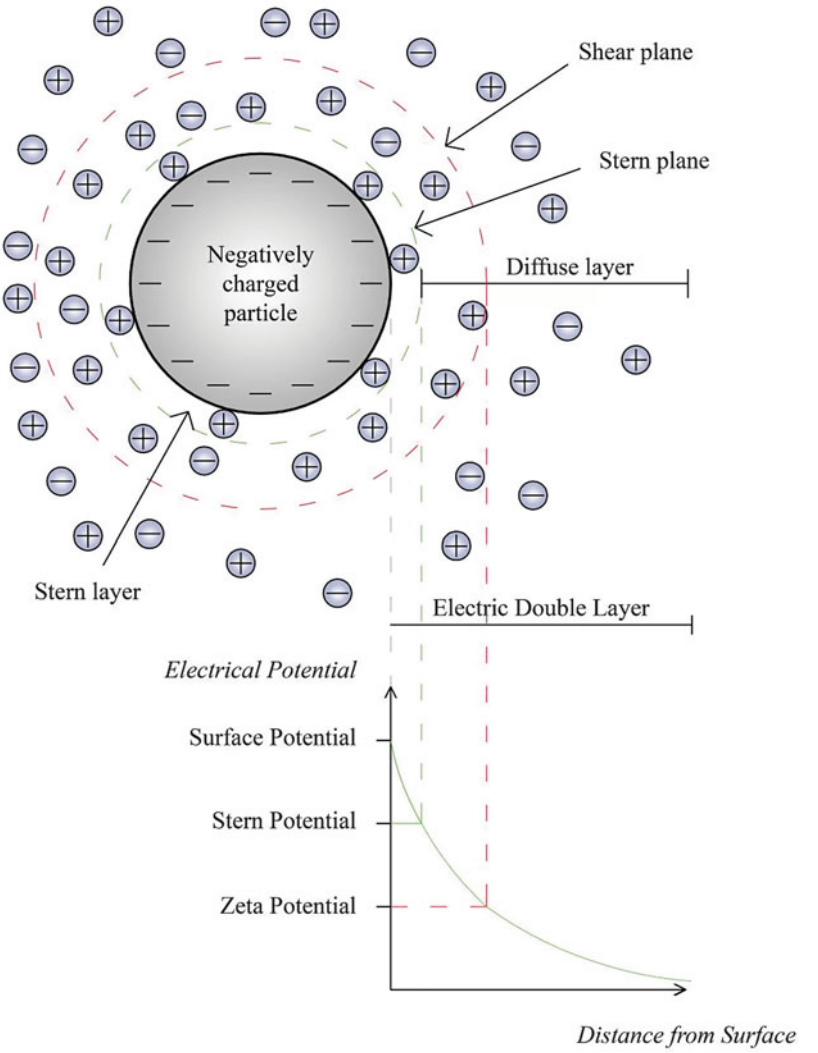

Fig. 10.1 Schematic of the Electrical Double Layer with an electrical potential graph for reference

or by the adsorption of ions from solution onto a previously uncharged surface. The final surface charge is balanced by an equal but oppositely charged region of counter-ions, some of which are bound, usually transiently, to the surface while others form an atmosphere of ions in rapid thermal motion close to the surface, known as the diffuse electrical double layer (EDL). The EDL model (Fig. 10.1) is used to visualise the ionic environment in the vicinity of a charged colloid and explains how the electrostatic repulsive force occurs. Ions of the same sign as the

charged surface are referred to as co-ions and those of an opposite sign are called counter-ions.

Attraction from the charged colloidal surface causes some of the counter-ions to form a firmly attached layer around the surface of the colloid; this layer of counter-ions is known as the *Stern layer*. The stern layer can be modelled using a Langmuir isotherm, which describes the formation of a monolayer. In this instance we have a monolayer of mainly counter-ions at the surface whose population is a function of the electrostatic potential (as well as chemical interactions). If we define the surface potential as ψ_0 then the potential at the stern plane is ψ_σ due to the effect of the adsorbed ions.

Beyond the stern plane additional counter-ions are still attracted by the colloidal surface charge, but now they are repelled by the Stern layer as well as by other positive ions that are also approaching the colloid due to thermal motion. This dynamic equilibrium between diffusion and electrostatics results in the formation of a *diffuse layer* of counter-ions. They have a high concentration near the surface which gradually decreases with distance, until it reaches the value of the counter-ion concentration in the solution. In a similar, but opposite, fashion there is a lack of co-ions in the neighbourhood of the surface, because they are repelled by the negative colloid. Their concentration will gradually increase with distance, as the repulsive forces of the colloid are screened out by the counter-ions, until the value of the co-ion concentration in the solution is reached.

The diffuse layer can be visualised as a charged atmosphere surrounding the colloid. The charge density at any distance from the surface is equal to the difference in concentration of positive and negative ions at that point. Charge density is greatest near the colloid and gradually diminishes towards unity as the concentration of positive and negative ions merge together. Within this diffuse layer the shear plane separates the mobile fluid from fluid that remains attached to the surface. The electric potential at this plane is called the electrokinetic potential or *zeta potential* (ζ). Although the position of the shear plane is not well defined (approximately three times the radius of a solvated ion), the zeta potential can be easily measured using electrokinetic techniques. The zeta potential can be used to evaluate the stern potential, assuming that approximately $\zeta \approx \psi_\sigma$.

In any medium containing free charges (for example water containing free ions in solution) all electrostatic fields become screened due to the polarisation (displacement) of these charges. A screened electric field decays approximately exponentially with distance x according to $e^{-\kappa x}$ where κ is the Debye–Hückel parameter which is measured in length^{-1} (10.1). The Debye–Hückel parameter characterises the decay of the potential with the distance from the surface. The Debye screening length (κ^{-1}) is a term used to describe the characteristic length or "thickness" of the EDL.

$$\kappa = \left(\frac{\sum_i \rho_{\infty i} e^2 z_i^2}{\varepsilon_0 \varepsilon k_B T} \right)^{\frac{1}{2}} \tag{10.1}$$

where $\rho_{\infty i}$ is the ionic concentration of ions i in the bulk, e is the electronic charge constant, z_i is the valency of ion i, ε_0 is the electric constant, ε is the relative static permittivity of the medium, T is the system's absolute temperature and k_B is the Boltzmann constant. It is interesting to note that, other than some fundamental constants, the Debye length depends only on the temperature and the bulk electrolyte concentration. As such Debye lengths for known electrolyte concentrations can be quickly evaluated, for example, the Debye length of NaCl at 25°C is $1/\kappa = 0.304/\sqrt{[\text{NaCl}]}$ nm where [NaCl] is the molecular concentration of the electrolyte, in this case sodium chloride. At low surface potentials (<25 mV) the potential of the EDL becomes proportional to the surface change density, and can be calculated as a function of the distance away from the stern layer as $\psi(x) \approx \psi_\sigma e^{-\kappa x}$.

10.1.4 DLVO Theory

Colloidal particle–particle interactions are described using the Derjaguin–Landau–Verwey–Overbeek (DLVO) [34] theory. The DLVO model combines the basic forces governing colloidal particles in suspension and it is primarily based on the relationships of long-range repulsive electrostatic forces and short-range attractive forces from the van der Waals interactions.

The stability of a particle in solution is dependent upon its total potential energy function V_T. DLVO theory assumes that V_T is the balance of two competing contributions:

$$V_T = V_A + V_R \tag{10.2}$$

where V_A is the non-retarded van der Waals attractive potential and V_R the EDL repulsive potential. The attractive potential energy related to van der Waals force interactions as the separation distance, D, between spherical particles of radius R changes is given by

$$V_A = -\frac{AR}{12D} \tag{10.3}$$

The repulsive potential V_R becomes significant when two colloids approach each other and their double layers begin to interfere. It has a maximum value when they are almost touching and decreases to zero outside the EDL.

$$V_R = \left(\frac{64\pi k_B T R \rho_\infty \gamma^2}{\kappa^2}\right) e^{-\kappa D} \tag{10.4}$$

where ρ_∞ is the electrolyte concentration in the bulk, $\gamma = \tanh(ze\,\psi_0/4k_BT)$.

DLVO theory allows evaluations of the stability of a colloidal system to be determined by the sum of these attractive and repulsive forces that exist between

particles as they interact with each other. A system could have a primary minimum and primary maximum in the total interaction energy potential. The primary minimum is where the attractive interactions dominate over the repulsive interactions and, conversely, the primary maximum is where the repulsive interactions dominate over the attractive interactions. In order to reach the primary minimum the particles must exceed the primary maximum activation energy. Therefore if $V_{\mathrm{T}}^{\mathrm{MAX}} \gg k_{\mathrm{B}}T$ the particles will be in a stable colloidal state. In certain situations (e.g. high electrolyte concentrations decreases the Debye length, effectively reducing the extent and intensity of the repulsive electrostatic interactions between the colloidal particles), there is a possibility of a secondary minimum where a much weaker and potentially reversible aggregation between particles exists. At the secondary minimum $-V_{\mathrm{T}}^{\mathrm{SMIN}} \sim k_{\mathrm{B}}T$ so the net attractive energy is at best only slightly larger than the average thermal energy. The result of this is the formation of weak flocs, sufficiently stable not to be broken up by Brownian motion, but may dissociate under an externally applied force such as vigorous agitation.

More recently the standard DLVO model has been updated to incorporate the short-range Lewis acid–base (AB) interactions that account for electron acceptor/electron donor interactions which have a measurable effect within a few nm of separation distance. The extended DLVO or XDLVO theory also can encompass other non-DLVO interactions arising from solvation forces in aqueous systems, in particular hydration forces [35] due to the energy required to disrupt the hydrogen-bonding network formed by the binding of water molecules to hydrophilic surfaces and structuring. The hydration force is an oscillating repulsive force of periodicity roughly equal to the diameter of a water molecule that grows exponentially in magnitude. In the case of silica and mica it is believed to arise from strongly H-bonding surface groups such as hydrated ions or hydroxyl groups, which leads to the modification of the H-bonding network of liquid water adjacent to them.

10.1.5 Electrolyte Concentration Control over Interactions

Due to the dependence of the Debye length on the ion concentration of the suspension, modification of the electrolyte concentration can provide us with a mechanism by which we can directly control the colloidal particle interactions. As attractive van der Waals forces are dependent only on the separation of the particles/surfaces, at low electrolyte concentrations when Debye screening is minimal, long-range repulsions severely limit the extent of adsorption due to the extended double-layer of ions surrounding it [36]. At higher electrolyte concentrations, the reduction in the Debye length causes the distance over which effective interparticle and particle–surface repulsions occur to be reduced. This suppression of the effective range of the repulsive force allows particles to approach one another and other surfaces at closer ranges, facilitating more densely packed arrangements, thus attaining higher surface coverage per unit area [37].

10.1.6 Steric Interactions

As previously mentioned, in order to maintain the stable dispersed colloidal system, the repulsive forces must be dominant ($V_T^{MAX} \gg k_B T$). To achieve an effective repulsive force without the use of electrostatic potentials, steric repulsion potentials can be utilised. For colloidal stability the use of steric repulsion involves the application of a thermally diffuse interface of chain molecules (oligmer or polymer) attached at some point to the surface of the colloid dangling out into the solution where they are thermally mobile. On approach of an analogous colloidal particle the entropy of confining these dangling chains results in a repulsive entropic force referred to as the "steric" or "overlap" repulsion. This allows colloidal particles suspended in a non-polar medium to be stabilised against coagulation by the addition of a suitable polymer to the system adsorbing onto the colloidal particle surface and physically preventing the particle surfaces coming into close enough contact for attractive London–van der Waals forces to cause coagulation. Unlike electrostatic stabilisation, there are no long-range repulsive forces and the particles could be subject to attractive forces until the outer portions of the steric molecules contact each other. The magnitude of the repulsion depends on the molecular weight of the polymer chain, the coverage of the polymer on the surface of the colloid, the mechanism by which the polymer is attached to the surface (adsorbed or end-grafted) and the quality of the solvent (i.e. if the polymer is in a poor solvent will coil up and shrink).

10.2 Experimental

10.2.1 Atomic Force Microscopy

The atomic force microscope was first reported by Binnig, Quate and Gerber [38] of IBM in 1986 and followed on from their work on scanning tunnelling microscopy (STM) [39], for which they were awarded the Nobel Prize for Physics. It was suggested as a means of studying non-conducting surfaces on an atomic scale, combining the principles of the STM and a stylus profilometer, and imaging by effectively "feeling" the sample surface. Owing to its high resolution (sub-nm) and ease of use in ambient conditions or within liquids, it is the most suitable technique for the direct observation of nanoparticle assemblies on surfaces and it is used widely.

The major components of a modern AFM are given in Fig. 10.2. The most important part is the tip, which makes the physical contact with the surface of the sample. The tip is usually made of silicon or silicon nitride, which is harder and hence more wear resistant. Typically tips have a micrometer scale pyramidal shape with a nanometer size apex radius. The tip is connected to a cantilever which allows the tip to move in relation to the topography of the sample. A laser beam

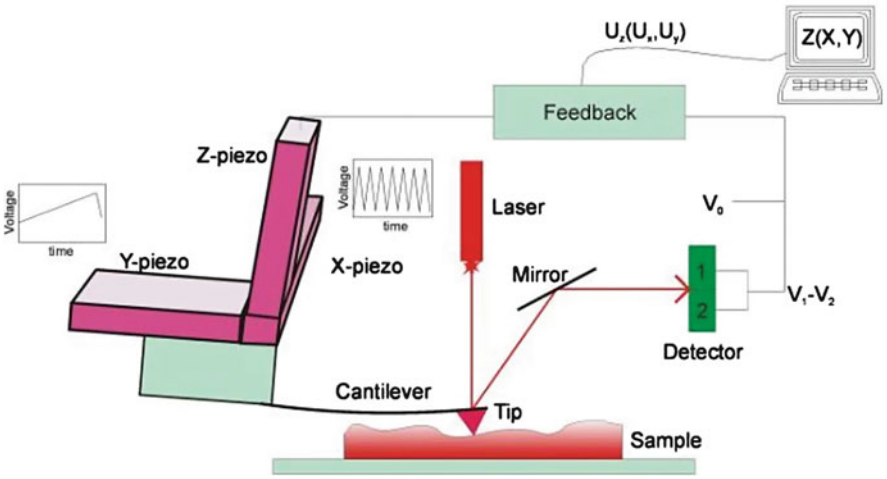

Fig. 10.2 Schematic diagram of an atomic force microscope

is directed onto the backside of the cantilever at the tip end and its reflection is directed onto a photodiode detector with four quadrants. The intensity of light in each quadrant gives information on the position of the cantilever and hence the tip. This information is then sent to a controller where a feedback mechanism registers a deflection of the cantilever and manipulates the displacement between the tip and the sample so that the deflection is constant. This is achieved by using piezoelectric crystals which can be utilised either as the sample stage or, in the case of our schematic, as the cantilever mount. When a voltage is applied across it, a controlled expansion/contraction occurs in the piezoelectric crystal. This motion is very reproducible and precise and allows the crystal to be deformed with the accuracy of atomic dimensions, giving an AFM the ability to perform very precise measurements of the sample topography. An image of the sample is achieved by raster scanning i.e. scanning line by line in the X and Y directions (again by using piezoelectric crystals to control the movement). The Z height data is calculated by taking the varying voltage applied to the Z axis piezoelectric crystal to maintain a constant deflection and scaling it with the known calibrated ratio of voltage to distance of the piezoelectric crystal.

This mode of operation is referred to as contact mode AFM: the cantilever/tip is maintained at a constant deflection and moved along the surface. This is one of the simplest methods of imaging using AFM techniques, however it has several drawbacks. The tip can exert considerable force on the sample surface. For soft samples such as polymers or biological specimens, the tip-force may cause an irreversible deformation of the surface so that the topography information becomes ambiguous or inaccurate. Similarly the frictional and lateral forces generated by the dragging of the tip also have a large magnitude. As such any weakly adsorbed material on the substrate will simply be dragged along the surface, rendering contact

mode ineffective for the imaging of delicate samples. To overcome such difficulties, it was suggested in 1987 that a non-contact (NC) mode [40] could be employed whereby the tip is not in constant contact with the surface but rather vibrates near the surface at its resonance frequency.

Intermittent contact (IC) mode AFM, was introduced in 1993 and differs only slightly from NC mode in that at the extreme of each oscillation the tip touches the surface very briefly. As the tip is brought close to the sample surface in IC mode, the characteristics of the cantilever vibration (e.g. amplitude, resonance frequency) change due to the tip-sample interaction and the feedback mechanism adjusts the tip-sample separation in order to maintain a constant amplitude of vibration. Another development of IC mode AFM gives the ability to detect shifts in phase angles of vibration when the oscillating cantilever interacts with the sample surface. The detection of phase angle shifts provides enhanced image contrasts for heterogeneous surfaces.

Given the size of the particles to be imaged in the present study, one of the most important AFM artefact effects to consider is tip convolution. This occurs due to the shape and the finite sharpness of the tip. The conical or pyramid or possibly spherical shape (at its very end) of a tip means that the side of the tip will make physical contact before the tip end, resulting in the imaged particle of radius R appearing wider than it really is, while the apparent height, $2R$, will be accurately measured as long as the particles are relatively sparsely distributed. Thus, it is important to accurately match the tip size to the topography of the sample. While we expect that some degree of blunting will occur throughout our experiments we endeavour to use clean, sharp tips for each set of experiments in order to avoid excessive convolution of the images that can be avoided if possible.

The most widely used substrate for AFM experiments is mica. Mica is a group of sheet silicate (phyllosilicate) minerals that feature highly perfect basal cleavage, due to the hexagonal sheet-like arrangement of its atoms. This property provides us with an easy to prepare, atomically flat substrate. For our experiments we will be using muscovite, $KAl_2Si_3AlO_{10}(OH, F)_2$, a high-aluminium mica. Upon cleavage along the basal plane, the exposed surface of the mica is a highly hydrophilic, negatively charged surface due to the non-equilibrium distribution of potassium ions across the cleaved surface, which reduces in time due to the attraction of oppositely charged contaminations.

10.3 Drying and Immersion Capillary Forces: The Emergence of Order

Lateral capillary forces between colloids in thin films occur when the particles are partially immersed in the liquid layer; this immersion capillary force causes the liquid surface surrounding the particle to deform as the liquid wets the surface of the colloidal particle. As a liquid film evaporates its height from the substrate shrinks until any colloidal particles within the film protrude through it. When this happens,

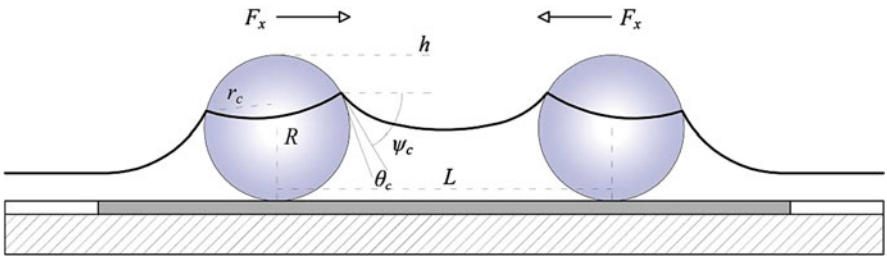

Fig. 10.3 Two spheres partially immersed in a liquid layer on a horizontal solid substrate. The deformation of the liquid meniscus and the particle separation distance gives rise to interparticle attraction

menisci form around the tops of the colloidal particles, generating an attractive force due to the deformation of the liquid surface and the induced asymmetry of the contact line at the surface of the particle. The magnitude of the force experienced between two neighbouring particles is dependent on several aspects including the separation distance of the particles, the radius of the three phase contact line and the contact angle of the meniscus. The latter two are dependent on the particle size and liquid film height.

Figure 10.3 gives a schematic representation of two spheres of radius R on a surface under the influence of capillary force F_x which can be approximated [27] as:

$$F_x \approx 2\pi\sigma r_c^2(\sin^2\psi_c)(1/L) \tag{10.5}$$

where σ is the surface tension of the liquid, r_c is the radius of the three-phase contact line at the particle surface ($r_c = [h(2R-h)]^{1/2}$), ψ_c is the mean meniscus slope angle at the contact line ($\psi_c = \arcsin(r_c/R)$–θ_c, where θ_c is the contact angle of the bulk liquid), h is the height of the liquid layer from the top of the particle ($2R$), and L is the distance between the particles. It is clear from the equation that the radius of the particle R plays a dominant role in dictating the capillary force experienced between the colloidal particles. Also notice that force exerted by the menisci is proportional to the inverse of the distance between the neighbouring particles (L). This means that the further the neighbouring particles are apart when the menisci forms between them, the less force the capillary action exerts between them.

These capillary forces are the main driving force behind creating self assembled 2D colloidal crystals. These are self assembled regular patterns that may extend to areas of mm^2 and are of great interest to the photonics industry due to their Bragg diffraction properties [24]. Early techniques used for constructing 2D crystal films were simply droplets of the colloidal suspension evaporated onto a substrate. Refinement of this process came with the utilisation of the meniscus line in evaporating liquids and by the 1990s the mechanism and governing forces of the 2D particle assembly had been clarified [26]. A two stage process was observed: (1) nucleus formation, under the action of attractive capillary immersion forces; and (2) crystal growth, through convective particle flux caused by the water evaporation from the already ordered array [24]. Control over this capillary force comes from

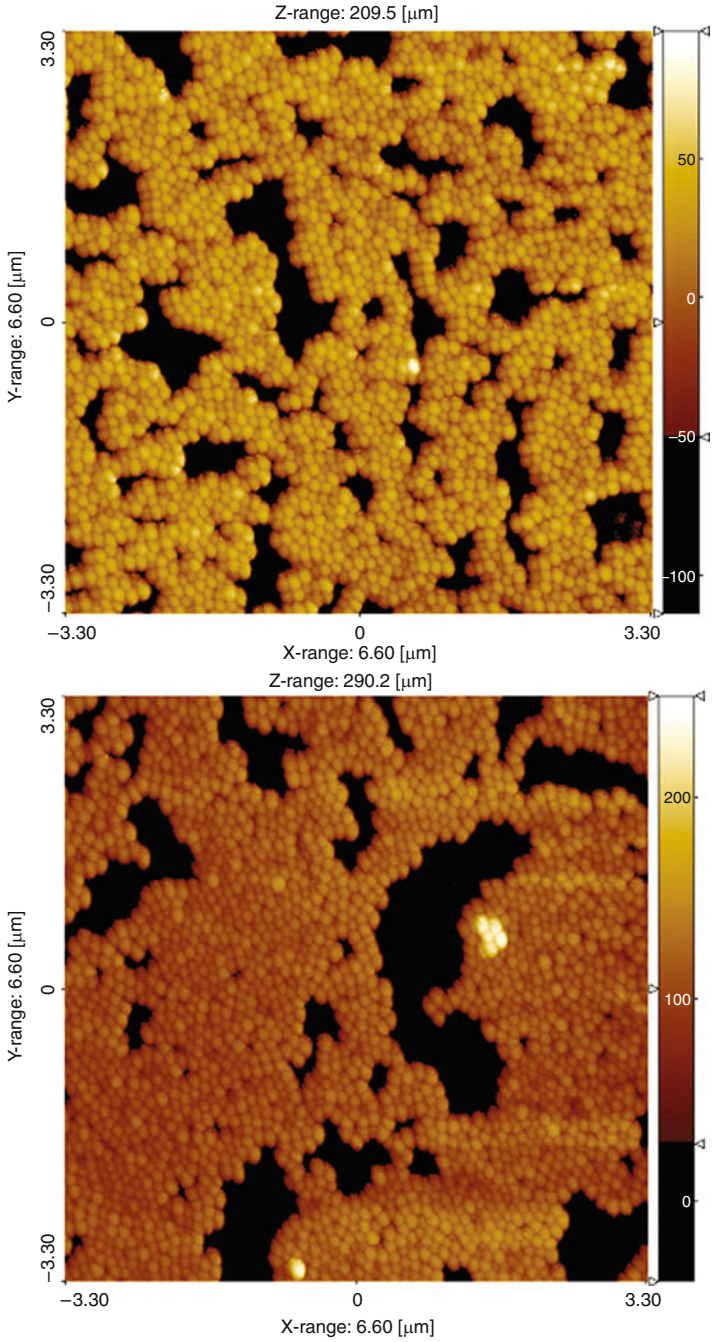

Fig. 10.4 $6.6 \times 6.6\,\mu m^2$ AFM images from different samples of 100 nm silica particles, diluted to 10% by volume. Freshly cleaved mica was submerged in the suspension and dried with a nitrogen stream

manipulation of the evaporation rate and the film meniscus. Dimitrov and Nagayama [26] demonstrated a now well-established technique for creating tuneable 2D crystalline films using a setup akin to a dip coating device, where the substrate is submerged into the colloidal suspension then withdrawn at a controlled rate. Other techniques include droplet application followed by tilting of the substrate [41], spin coating the colloidal suspension on the substrate [42] and the use of pre-patterned surfaces to create specific sites that are more energetically favourable to adsorb to. These techniques result in 2D crystalline films where either multidomain or one large single domain crystal is grown.

10.3.1 Crystalline Monolayers of Colloidal Silica on Mica

When suspended in water, silica particles [43] have a native negative charge on the surface due to the dissociation of silanol groups which allow them to maintain an even dispersion in favourable pH levels and avoid coagulation without the need for surface chemistry modification. The system of silica particles and mica gives us an opportunity to study self-assembly of nanoparticles on a substrate of the same charge (negative). While van der Waals forces are sufficient to provide adsorption for appropriate incubations times the repulsive electrostatic force enhances the lateral mobility. Such systems have not been sufficiently explored in current literature. They provide an alternative system for bottom up self assembly of

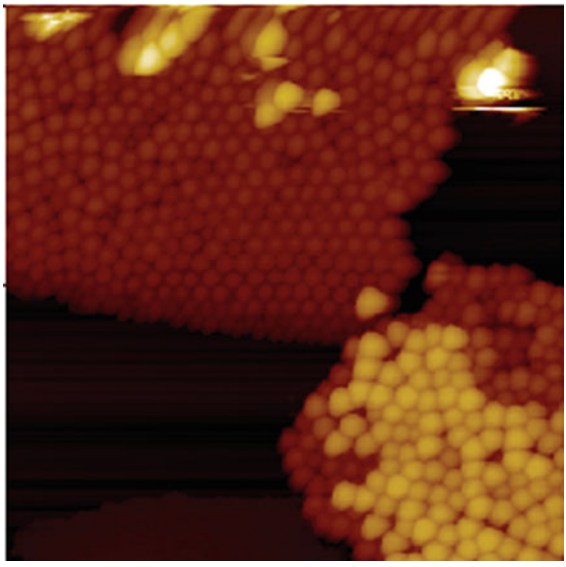

Fig. 10.5 $3.3 \times 3.3\,\mu m^2$ topography AFM scan with a colloidal crystalline monolayer area at the upper part of the image

colloidal nanoparticles. In Fig. 10.4 we show silica nanoparticles (Polysciences Inc., Baden-Württemberg, Germany) of diameter of ∼100 nm deposited on mica by dip coating and subsequent drying. The monolayer network observed is characteristic of the drying and dewetting process while the ordering (see also zoom in Fig. 10.5) is attained by crystal nucleus formation due to attractive capillary immersion forces and subsequent crystal growth via convective particle flux as the water evaporates. The repulsive electrostatic interactions between silica and mica (as they are both negatively charged) facilitate mobility along the surface.

10.4 Dewetting Effects: Self-Organisation

The crystalline structuring of colloidal particles has typically been the domain of some hundreds of nanometers to micrometer sized particles. Research into the self assembly of nanometer sized colloids has yielded some radically different particle structuring, such as 2D cellular structures. These are normally associated with dewetting phenomena found in thin liquid films that undergo rupture and coalescence into network structures. Martin et al. [44] carried out studies linking this, normally fluid, behaviour to other systems including nanocolloidal suspensions of gold nanoparticles of a few nanometers in diameter. They found striking resemblances in morphology and using Voronoï tessellation to calculate the distribution of particles on the surface of the samples were able to assess the degree of (dis)order within a system by comparing these results with those from Poisson distributed simulations.

Rabani et al. [45] demonstrated a model for drying mediated self assembly of nanoparticles that simulates remarkably well the behaviour of these complex fluids by including not only the relatively weak attractions between the particles themselves but also the dynamics of an evaporating solvent. Using their model they were able to show that varying the choice of solvent, particle size and thermodynamic state gave rise to various morphologies.

The dewetting phenomena can simply be described with the example of a new car left in the rain. The water droplets on the waxed surface do not coat the bodywork evenly, rather they coalescence into droplets on the surface. In effect the rain water "dewets" on the car panels. Generally dewetting describes the rupture of a thin liquid film on the substrate (either a liquid itself, or a solid) and the subsequent formation of droplets. Recent insights into the balance between short and long-range forces involved in dewetting phenomena resulted in Sharma and Reiter [46, 47] presenting the following four-stage dewetting process from experimental observations: (1) rupture of the thin film; (2) expansion and coalescence of holes to form polygonal "cellular" patterns; (3) fingering instability of hole rims during hole expansion witnessed only on low wettability surfaces (can also occur after stage 4); (4) disintegration of liquid ridges forming the polygon into spherical drops due to Rayleigh instability.

Seemann, Herminghaus and Jacobs [48] provided a clarification of the distinction between stable, unstable and metastable films using the effective interface potential, $\Phi(h)$, which is defined as the excess free energy (per unit area) it takes to bring two interfaces from infinity to a certain distance, h. In the case of a dewetting film, the two interfaces involved are the solid/liquid interface and the liquid/air interface, and h is the initial thickness of the liquid film. By consequence $\Phi \rightarrow 0$ as $h \rightarrow \infty$. In a scenario where $\Phi(h) > 0$ the global minimum lies at infinite film thickness. In this case the liquid film is termed stable. If the global minimum of $\Phi(h)$ occurring at a point h^* then the free energy $\Phi(h)$ of the film possesses a negative curvature at the starting thickness, h_o, i.e. $\Phi''(h_o) < 0$, the system can gain energy by allowing the film thickness to reach h^*. If the initial film thickness is greater than h^* then the film will try to attain an equilibrium film thickness of h^* causing localised thinning in the film that will ultimately lead to rupturing and subsequent dewetting. Thus from infinity to h^* the film is unstable against *spinodal* dewetting. Spinodal Dewetting [49] is triggered by spontaneous amplification of capillary waves within the film caused by thermal fluctuations and is usually characterised by a bicontinuous structure of the phase separation morphology which can be identified by 2D-FFT analysis of the morphology. Finally, there is a third scenario where a system is metastable; that is at low film thicknesses where $\Phi''(h_o) < 0$, spinodal dewetting can occur, but at larger film thicknesses it is stable against spinodal dewetting.

A second dewetting mechanism known as nucleation dewetting [50] can cause dewetting to occur on stable, metastable and unstable films either by nuclei defects such as dust particles/surface heterogeneities (heterogeneous) or by localised thermal instabilities (homogeneous). Nucleation dewetting can occur in parallel or at a different time frame to spinodal dewetting as the two processes are independent.

For heterogeneous nucleation, because the dewetting is initiated by surface defects the initial surface ruptures occur over a small time frame. Unlike spinodal dewetting however a characteristic length in the morphology does not exist. Homogeneous nucleation differs in that it has a continuous breakout of holes on the surface throughout the time frame, caused by the local fluctuations in thermal energy allowing the liquid to overcome the potential barrier for nucleation of a dry spot, leading to the formation of a hole. There are usually time and size differences between the different dewetting mechanisms.

10.4.1 Dewetting Structures of Colloidal Magnetite Nanoparticles on Mica

In Fig. 10.6, we present typical images of colloidal deposits after evaporation of a colloidal magnetite *n*-heptane suspension [51]. In this case the nanoparticles have been much smaller: diameter ~10 nm. The solvent film ruptured at a higher thickness and before immersion capillary forces were able to be exerted on the individual nanoparticles. The end result was the nanoparticles to follow the solvent

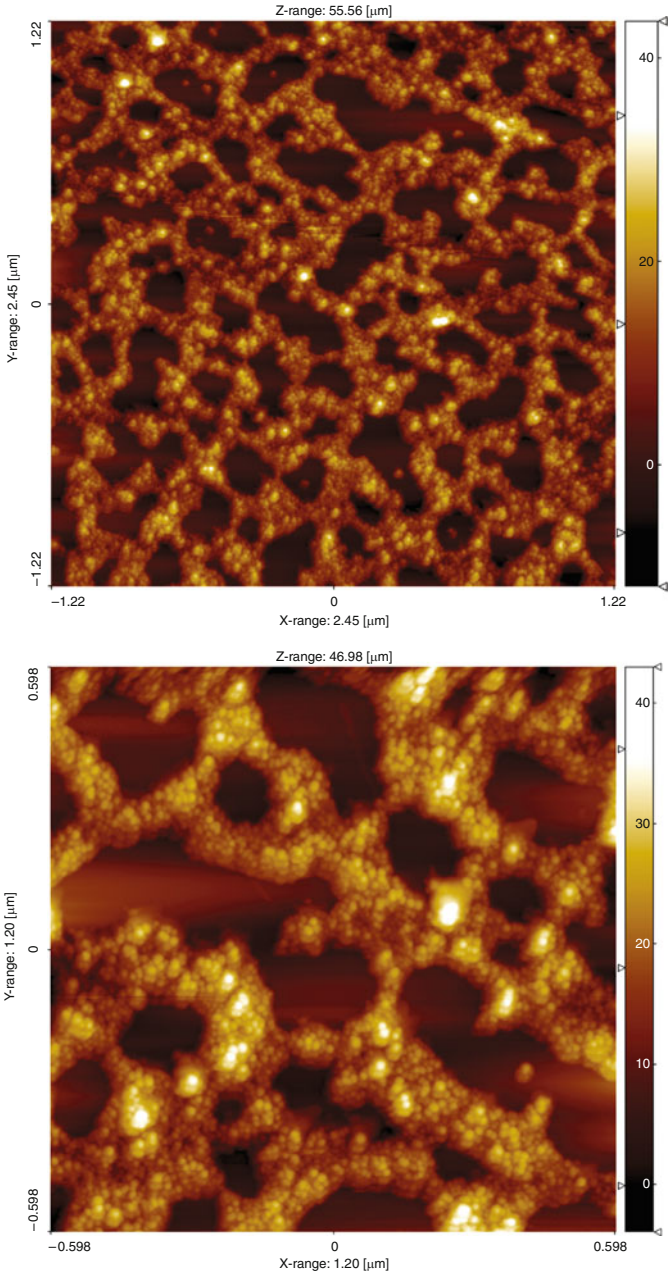

Fig. 10.6 AFM topography images (top $2.45 \times 2.45\,\mu m^2$, bottom $1.20 \times 1.20\,\mu m^2$) of deposits on mica after solvent evaporation from dilute magnetite nanoparticle suspensions

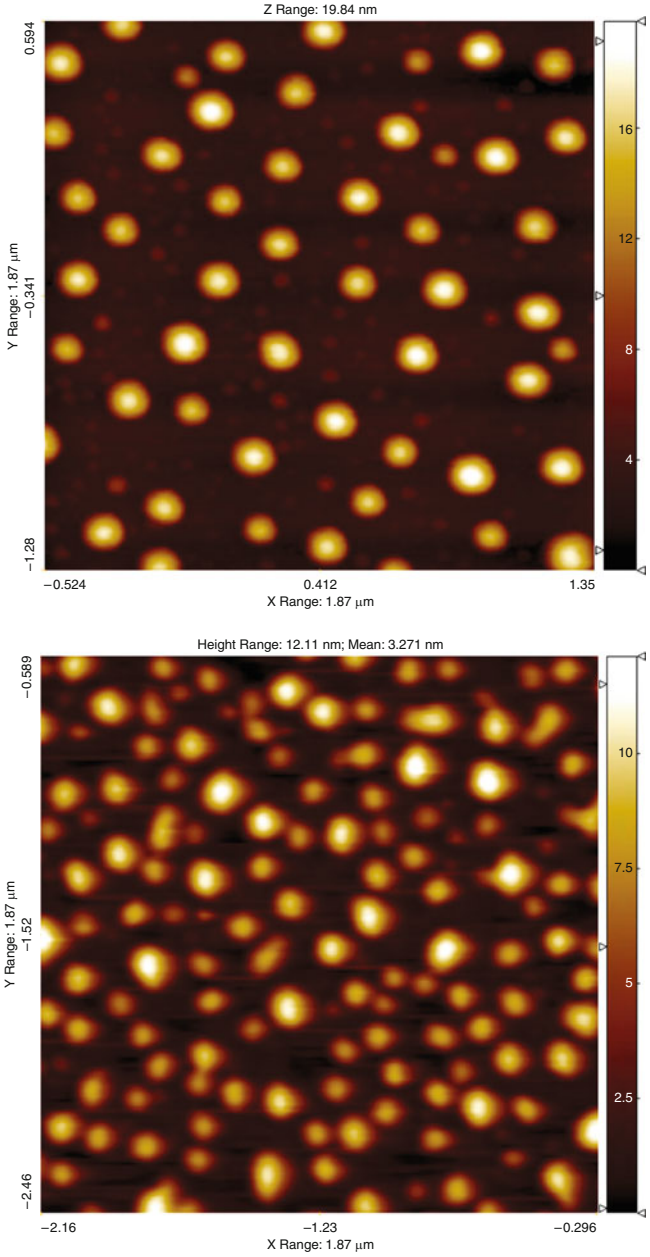

Fig. 10.7 AFM topography images ($1.87 \times 1.87\,\mu m^2$) of 59-arm star polymers adsorbed on mica. Top: after 1,080 min, bottom: after 3,600 min immersion time in the toluene solution

dewetting instability en mass and to create an irregular (non-crystalline) multilayer network (see zoom in Fig. 10.6). It is worthwhile noting the profound difference in the fine structure of 100 nm particles (Fig. 10.5) and 10 nm particles (Fig. 10.6). The 'premature' rupture of the film does not allow the immersion capillary forces to develop and create order in the case of the smaller particles. Nevertheless, there is still the cellular network formation which is still evidence for self-organisation resulting from the dewetting process.

10.4.2 Adsorption and Self-Assembly of Soft Colloid Nanoparticles on Mica

Figure 10.7 presents AFM images of a soft nanoparticle system: mica substrates dip-coated in a 59-arm polybutadiene star polymer toluene solution [52, 53]. Star polymers (macromolecules with homopolymer arms covalently joined to a dendritic core) with a large number arms (high functionality) behave like colloid particles owing to the fact that the osmotic pressure within the star increases with the star polymer functionality, which in turn makes the star polymer harder, preventing interpenetrations between different star polymers [54, 55]. The star polymers of such functionality behave to some extent like colloid particles stabilised by steric repulsions that develop within a good solvent (toluene in this case). In solution but also in dry state they keep to some extent their 3D shape [52, 53], they do not fuse and keep their individuality even at high surface densities (Fig. 10.7). However, it is quire remarkable that they do not seem to be affected by capillary forces and dewetting instabilities even though their interactions with the surface are relatively weak at the monomer level (just dispersion forces as polybutadiene is apolar). These polymer particles possess surface mobility but the final position of the particles are determined solely by particle–particle interactions on the surface when in the solution (mainly steric repulsions in this case); the AFM images are essentially snapshots of the polymer particle position just before drying [52, 53]. This can be an advantage for self assembly allowing more complex interactions (than capillary forces) to take place and thus more complex structures to develop on the surface (while in solution) without having the complication of solvent instabilities during drying.

10.5 Conclusions

We have shown that colloidal nanoparticles can be used for nanopatterning of solid surfaces via the self-assembly route. This process provides an inexpensive and facile methodology for the fabrication of large areas of nanoscale patterns. However, the mechanisms that govern the self-assembly behaviour are complex and in many cases competing. We have provided examples to demonstrate these

factors in model systems. While relatively large nanoparticles (∼100 nm) can form colloidal crystalline monolayers via the immersion capillary forces, the situation becomes very different at diameters of 10 nm, where dewetting effects dominate. However, neither of these mechanisms seem to dominate the behaviour of soft colloidal nanoparticles (high functionality star polymers) which self-assemble based purely on molecular interactions (steric repulsions) within the solution even when they are weakly adsorbed on the substrate (via van der Waals forces). Such systems could offer opportunities for the finetuning of interactions to fabricate more complex nanopatterns.

References

1. J.H. Fendler, Chem. Mater. **13** 3196–3210 (2001)
2. J. Texter, M. Tirrell, AIChE J. **47** 1706–1710 (2001)
3. G.M. Whitesides, B. Grzybowski, Science **295** 2418–2421 (2002)
4. S.C. Glotzer, M.J. Solomon, N.A. Kotov, AIChE J. **50** 2978–2985 (2004)
5. C.P. Martin, M.O. Blunt, E. Vaujour, A. Fahmi, A. D'Aléo, L. De Cola, F. Vögtle, P. Moriarty, Chapter 1, Self-Organised Nanoparticle Assemblies: A Panoply of Patterns, In: N. Krasnogor, S. Gustafson, D.A. Pelta and J.L. Verdegay, Editors, Studies in Multidisciplinarity, Elsevier, Oxford, 2008, Volume 5, Systems Self Assembly: Multidisciplinary Snapshots, Pages 1–20
6. G.M. Whitesides, B. Grzybowski, Science **295** 2418–2421 (2002)
7. M. Shimomura, T. Sawadaishi, Curr. Opin. Colloid Interface Sci. **6** 11–16 (2001)
8. D. Mijatovic, J.C.T. Eijkel, A. van den Berg, Lab Chip **5** 492–500 (2005)
9. S.H. Im, Y.T. Lim, D.J. Suh, O.O. Park, Adv. Mater. **14** 1367–1369 (2002)
10. O.D. Velev, E.W. Kaler, Langmuir **15** 3693–3698 (1999)
11. P. Hanarp, D.S. Sutherland, J. Gold, B. Kasemo, Colloids Surf. A Physicochem. Eng. Asp. **214** 23–36 (2003)
12. P. Guyot-Sionnest, Compt. Rend. Phys. **9** 777–787 (2008)
13. M. Qhobosheane, S. Santra, P. Zhang, W.H. Tan, Analyst **126** 1274–1278 (2001)
14. M.S. Romero-Cano, A. Martin-Rodriguez, G. Chauveteau, F.J. de las Nieves, J. Colloid Interface Sci. **198** 266–272 (1998)
15. J.Z. Xue, E. Herbolzheimer, M.A. Rutgers, W.B. Russel, P.M. Chaikin, Phys. Rev. Lett. **69** 1715–1718 (1992)
16. M. Elimelech, C.R. Omelia, Langmuir **6** 1153–1163 (1990)
17. Z. Adamczyk, J. Colloid Interface Sci. **229** 477–489 (2000)
18. Z. Adamczyk, L. Szyk, Langmuir **16** 5730–5737 (2000)
19. Z. Adamczyk, B. Siwek, M. Zembala, Colloids Surf. A Physicochem. Eng. Asp. **62** 119–130 (1992)
20. N. Rana, S.T. Yau, Nanotechnology **15** 275–278 (2004)
21. S. Maenosono, T. Okubo, Y. Yamaguchi, J. Nanopart. Res. **5** 5–15 (2003)
22. N. Samid-Merzel, S.G. Lipson, D.S. Tannhauser, Physica A **257** 413–418 (1998)
23. J. Aizenberg, P.V. Braun, P. Wiltzius, Phys. Rev. Lett. **84** 2997–3000 (2000)
24. P.A. Kralchevsky, N.D. Denkov, Curr. Opin. Colloid Interface Sci. **6** 383–401 (2001)
25. P.A. Kralchevsky, K. Nagayama, Langmuir **10** 23–36 (2002)
26. A.S. Dimitrov, K. Nagayama, Langmuir **12** 1303–1311 (1996)
27. N.D. Denkov, O.D. Velev, P.A. Kralchevsky, I.B. Ivanov, H. Yoshimura, K. Nagayama, Langmuir **8** 3183–3190 (1992)
28. K. Nagayama, Colloids Surf. A Physicochem. Eng. Asp. **109** 363–374 (1996)

29. Z. Adamczyk, *Particles at Interfaces, Volume 9: Interactions, Deposition, Structure*, (Academic Press, Amsterdam, Oxford, 2006)
30. D.H. Everett, *Basic Principles of Colloid Science* (Royal Society of Chemistry, London, 1988)
31. J. Goodwin, *Colloids and Interfaces with Surfactants and Polymers: An Introduction* (John Wiley, Chichester, 2004)
32. R.J. Hunter, *Foundations of Colloid Science* (Oxford University Press, Oxford, 2001)
33. J.N. Israelachvili, *Intermolecular and Surface Forces* (Academic Press, New York, 1992)
34. B. Derjaguin, L.D. Landau, Acta Physicochim. (USSR) **14** 633–662 (1941)
35. R.M. Pashley, J. Colloid Interface Sci. **80** 153–162 (1981)
36. R. Rajagopalan, R.Q. Chu, J. Colloid Interface Sci. **86** 299–317 (1982)
37. C.A. Johnson, A.M. Lenhoff, J. Colloid Interface Sci. **179** 587–599 (1996)
38. G. Binnig, C.F. Quate, C. Gerber, Phys. Rev. Lett. **56** 930 (1986)
39. G. Binnig, H. Rohrer, C. Gerber, E. Weibel, Phys. Rev. Lett. **50** 120 (1983)
40. Y. Martin, C.C. Williams, H.K. Wickramasinghe, J. Appl. Phys. **61** 4723–4729 (1987)
41. R. Micheletto, H. Fukuda, M. Ohtsu, Langmuir **11** 3333–3336 (1995)
42. P. Jiang, T. Prasad, M.J. McFarland, V.L. Colvin, Appl. Phys. Lett. **89**011908–011903 (2006)
43. R.K. Iler, *The Chemistry of Silica: Solubility, Polymerization, Colloid and Surface Properties, and Biochemistry* (Wiley, New York, 1979), pp. xxiv, 866
44. C.P. Martin, M.O. Blunt, P. Moriarty, Nano Lett. **4** 2389–2392 (2004)
45. E. Rabani, D.R. Reichman, P.L. Geissler, L.E. Brus, Nature **426** 271–274 (2003)
46. A. Sharma, G. Reiter, J. Colloid Interface Sci. **178** 383–399 (1996)
47. A. Sharma, R. Verma, Langmuir **20** 10337–10345 (2004)
48. R. Seemann, S. Herminghaus, K. Jacobs, Phys. Rev. Lett. **86** 5534–5537 (2001)
49. R. Xie, A. Karim, J.F. Douglas, C.C. Han, R.A. Weiss, Phys. Rev. Lett. **81** 1251–1254 (1998)
50. U. Thiele, M.G. Velarde, K. Neuffer, Phys. Rev. Lett. **87** 016104 (2001)
51. K.J. Mutch, V. Koutsos, P.J. Camp, Langmuir **22** 5611–5616 (2006)
52. E. Glynos, A. Chremos, G. Petekidis, P.J. Camp, V. Koutsos, Macromolecules **40** 6947–6958 (2007)
53. A. Chremos, E. Glynos, P.J. Camp, V. Koutsos, Soft Matter **6** 1483–1493 (2010)
54. D. Vlassopoulos, G. Fytas, T. Pakula, J. Roovers, J. Phys.: Condens. Matter **13** R855–R876 (2001)
55. C.N. Likos, Phys. Rep. **348** 267–439 (2001)